

A mechanistic examination of salting out in proteinpolymer membrane interactions

Nicholas A. Moringo^a, Logan D. C. Bishop^a, Hao Shen^{a,1}, Anastasiia Misiura^a, Nicole C. Carrejo^a, Rashad Baiyasi^b, Wenxiao Wang^b, Fan Ye^b, Jacob T. Robinson^{b,c}, and Christy F. Landes^{a,b,d,e,2}

^aDepartment of Chemistry, Rice University, Houston, TX 77251; ^bDepartment of Electrical and Computer Engineering, Rice University, Houston, TX 77251; ^cDepartment of Bioengineering, Rice University, Houston, TX 77251; ^dSmalley-Curl Institute, Rice University, Houston, TX 77251; and ^eDepartment of Chemical and Biomolecular Engineering, Rice University, Houston, TX 77251

Edited by Catherine J. Murphy, University of Illinois at Urbana-Champaign, Urbana, IL, and approved October 1, 2019 (received for review June 7, 2019)

Developing a mechanistic understanding of protein dynamics and conformational changes at polymer interfaces is critical for a range of processes including industrial protein separations. Salting out is one example of a procedure that is ubiquitous in protein separations yet is optimized empirically because there is no mechanistic description of the underlying interactions that would allow predictive modeling. Here, we investigate peak narrowing in a model transferrin-nylon system under salting out conditions using a combination of single-molecule tracking and ensemble separations. Distinct surface transport modes and protein conformational changes at the negatively charged nylon interface are quantified as a function of salt concentration. Single-molecule kinetics relate macroscale improvements in chromatographic peak broadening with microscale distributions of surface interaction mechanisms such as continuoustime random walks and simple adsorption-desorption. Monte Carlo simulations underpinned by the stochastic theory of chromatography are performed using kinetic data extracted from single-molecule observations. Simulations agree with experiment, revealing a decrease in peak broadening as the salt concentration increases. The results suggest that chemical modifications to membranes that decrease the probability of surface random walks could reduce peak broadening in full-scale protein separations. More broadly, this work represents a proof of concept for combining single-molecule experiments and a mechanistic theory to improve costly and time-consuming empirical methods of optimization.

single-molecule tracking | membrane chromatography | salting out | stochastic theory of chromatography

Protein separation and purification are the dominant expenses in biological drug development, largely because they are optimized empirically (1-3). Mechanistic insight into protein separations would allow the predictive optimization of macroscale separations (4-6) and broadly impact everyday healthcare products (7, 8) and biosensing devices (9-13). A common process in protein separations is "salting out," in which high salt concentrations are introduced to the mobile phase to improve elution efficiency (14, 15). Salting out is thought to aid in separations by altering protein-stationary phase interactions through ionic shielding (16, 17) and/or precipitating proteins from the mobile phase as predicted by the Hofmeister series, leading to faster elution (18–20). Acquiring micro- and nanoscale details about protein/stationary phase interactions during salting out is crucial because the ionic conditions can be related to macroscale peak broadening in protein separations (21-24). Understanding the dynamic changes occurring at separation interfaces is of critical societal importance, as recently reported by the National Academy of

Structure–function relationships between target proteins and the stationary phase under salting out conditions are not well understood and are experimentally challenging to quantify in situ (14, 15). Common methods for monitoring protein–surface interactions include surface plasmon resonance (26), isothermal titration calorimetry (27), and atomic force microscopy (28).

Although these experimental techniques provide new insight into complex protein-polymer interactions, they suffer from ensemble averaging and lack high spatiotemporal resolution necessary to develop a physiochemical mechanism of protein-stationary phase interactions. Moreover, proposed models extracted from these techniques likely oversimplify the underlying mechanism of interfacial adsorption-desorption, surface diffusion, and surfaceinduced protein unfolding effects (26, 27). Single-molecule microscopy is well suited to directly visualize protein mass transport at a wide array of complex interfaces one molecule at a time with a high spatiotemporal resolution (29-34). However, atomistic details of protein surface domains and/or substrate chemistries interacting during protein physisorption is not resolved in comparison to atomistic modeling techniques (35). Heterogeneous protein surface kinetics and transport can be quantified in experimentally challenging systems (36, 37) as a result of advancements in single-molecule tracking algorithms (38, 39), point spread function engineering techniques (40-43), and the increased sensitivity of scientific cameras (29).

Herein, total internal reflection fluorescence (TIRF) widefield single-molecule tracking is used in combination with ensemble

Significance

Membrane-based protein separations are utilized broadly, and increasingly, to purify proteins for research and biopharmaceuticals. Like all steps in the purification process, the salt concentration is adjusted empirically in the mobile phase to elute a desired component of a protein mixture. There is insufficient quantitative description about the salting out process to allow for predictive optimization. By quantifying the interactions and kinetics of single proteins at the surface of a membrane as salt concentration is increased, we relate mechanistic nanoscale observables to an improvement in the peak broadness observed in real separations. This result suggests that simulations, informed by small-scale single-molecule observations, could be used to optimize separation conditions, leading to more efficient separations.

Author contributions: N.A.M., L.D.C.B., H.S., N.C.C., and C.F.L. designed research; N.A.M., L.D.C.B., H.S., A.M., N.C.C., and C.F.L. performed research; N.A.M., A.M., N.C.C., R.B., W.W., F.Y., and J.T.R. contributed new reagents/analytic tools; N.A.M., L.D.C.B., N.C.C., R.B., and W.W. analyzed data; and N.A.M., L.D.C.B., N.C.C., and C.F.L. wrote the paper.

The authors declare no competing interest.

This article is a PNAS Direct Submission.

Published under the PNAS license.

Data deposition: All scripts used to run the simulations and code bases are available for download at https://github.com/LandesLab?tab=repositories. All data presented in figures are available in an online directory at https://rice.box.com/s/n3cmfg5ji0lmw4fxt5gsqnzxho5rxfy1.

¹Present address: Department of Chemistry and Biochemistry, Kent State University, Kent, OH 44244.

²To whom correspondence may be addressed. Email: cflandes@rice.edu.

This article contains supporting information online at www.pnas.org/lookup/suppl/doi:10. 1073/pnas.1909860116/-/DCSupplemental.

First published October 28, 2019.

of at FONDBEN LIBRARY MS 235 on May 26 20

fast protein liquid chromatography (FPLC) to relate tracking observables to ensemble elution profiles. Additionally, circular dichroism (CD) spectroscopy is utilized to quantify structural changes of proteins at the stationary phase support and relate to TIRF and FPLC results. TIRF single-molecule tracking has been recently shown to reveal interfacial protein dynamics on a range of surfaces, including natural and synthetic polymers (44–48), and is ideal for measuring interfacial dynamics as it intrinsically suppresses background signal from emitters diffusing in the bulk solution. TIRF microscopy has been applied in many other systems including nanoparticle catalysis (49–51), DNA hybridization kinetics (52–54), and protein transport in live cells (54, 55). These examples also highlight the robust nature of single-molecule tracking for investigating multiplexed and heterogeneous systems (56, 57).

The dynamics of single transferrin proteins, a well-studied cancer therapeutic target (58, 59), at the interface of nylon 6,6 is used to examine the mechanistic origin of changes in chromatographic peak width during salting out in FPLC. CD results lend insight into the structural changes induced to transferrin at the nylon interface during salting out and are related to singlemolecule tracking and FPLC observables. Increasing salt concentration is used to emulate salting-out conditions used in membrane chromatography. Nylon is chosen as a stationary phase material as it is commonly used in protein membrane separations and is a known hydrophilic antifouling surface (60, 61). Membrane-based separations have garnered recent interest given the reduced mass transfer resistance, increased surface area for adsorption, and lower column costs in comparison to traditional bead-packed columns (62). Additionally, nylon is a chemically robust and optically transparent polymer stable under laser illumination (40, 63) and utilized in many consumer products (64). Surface transport modes and kinetics of transferrin are quantified at the singlemolecule level and used to explain the reduction of peak broadening observed in ensemble separations. Single-molecule kinetics further inform Monte Carlo simulations that agree with FPLC results, predicting peak narrowing at higher salt concentrations. Single-molecule observables link ensemble separations based on a mechanism that is supported by simulation.

Materials and Methods

Single-Molecule Tracking. A home-built wide-field epifluorescence microscope (Zeiss body, tube lens f = 165 mm) is used for all single-molecule experiments. TIRF excitation of fluorescently labeled transferrin is achieved with a continuous-wave 532-nm diode laser (Compass 315M-100SL; Coherent) focused at the edge of a high-numerical-aperture oil immersion objective (numerical aperture = 1.45, 100×, Alpha Plan-Fluar; Carl Zeiss) resulting in a critical angle of roughly 78°. TIRF excitation produces an exponentially decaying evanescent field that propagates from the nylon-buffer interface roughly 85 nm into the bulk solution (65), thus only exciting transferrin molecules located near the nylon surface. The refractive index of nylon (1.58) closely matches glass (1.51), in contrast to the refractive index of aqueous Hepes buffer used in the protein dilutions (1.33) (37). Refractive index mismatch at the buffer-nylon interface meets the TIRF condition. Experimental confirmation of the TIRF condition at the buffer-nylon interface was previously shown (37). Evanescent field excitation improves the signal-to-noise ratio by suppressing excitation of transferrin molecules in the bulk solution. Excitation power density at the hylon interface is 0.10 kW/cm² for all single-molecule acquisitions. Collected fluorescent light is magnified by 2.5x and is filtered using a dichroic filter (z532/rpc633; Chroma), notch filter (HPNF-532; Kaiser), and band-pass filter (ET585; Chroma), ensuring all laser light is removed from the final image. Images are collected on an electron-multiplying charge-coupled device (iXon 897; Andor) operated at -70 °C. All movies are collected with an integration time of 50 ms and a gain of 300. A previously published tracking algorithm is used to track single molecules on the nylon interface and is explained in further detail in SI Appendix (39). A minimum of 10,000 transferrin trajectories are analyzed for each condition.

Nylon Film Preparation and Microfluidic Assembly. Borosilicate microscope coverslips (no. 1; Fisherbrand) are sonicated for 30 min in 200-mL baths of cleaning agents: soapy water (Liquinox 2%), deionized water (>1M Ω -cm), methanol (ACS grade; Sigma), and acetone (ACS grade; Sigma) sequentially. Coverslips are then chemically etched in a base piranha solution heated at 80 °C for 20 min and then rinsed under a stream of deionized water prior to drying under a stream of nitrogen (Ultra Pure; Airgas).

Nylon 6,6 pellets (zeta potential -21 ± 1 mV; Sigma; *SI Appendix*) are dissolved in formic acid (ACS grade; Sigma) to produce a 1.5 wt/wt % solution; 100 μ L of the nylon solution is drop-cast on a coverslip and spin-coated at 3,000 rpm (SPI KW-4A) for 1 min. A dilute concentration of gold nanorods (50 \times 100 nm; Nanopartz) are spin-coated on the nylon film to act as fiducial markers. Microfluidic assemblies (Hybriwell Chamber; Grace BioLabs) are then attached to the nylon interface with tubes (0.03-inch internal diameter; Scientific Commodities) attached at the inlet and outlet to supply a constant solution of 100 pM labeled transferrin at 50 μ L/min in 10 mM Hepes buffer (pH = 7.2).

Nylon Film Ellipsometry. Nylon film thickness is quantified (129 \pm 0.3 nm) using ellipsometry (7109-C370B; Gaertner; *SI Appendix*, Fig. S1). Nylon films are spin-coated on clean silicon wafers (100; Ted Pella) for ellipsometry measurements.

Fluorescent Protein Solution Preparation. Rhodamine B labeled transferrin (Nanocs) is dissolved in 10 mM Hepes buffer and is diluted to 100 pM for all single-molecule experiments presented in this work. Mass spectrometry confirms the purity and absence of contaminant proteins and/or free-dye molecules in the purchased protein powder (*SI Appendix*, Fig. S2).

Nylon Bead Preparation. A 1.5 wt/wt % formic acid solution of nylon 6,6 is sonicated for roughly 24 h and then slowly added to water under continuous stirring. The resulting precipitate is filtered using an 8-µm filter (Whatman) to remove large nylon aggregates.

Ensemble FPLC. Ensemble separations are conducted on a home-built FPLC system. Flow is controlled using a peristaltic pump (120 Series; Watson-Marlow) and absorbance is monitored at 280 nm using a UV detector (Spectrum Chromatography) and recorded on a digital recorder (365E; Hantek) controlled by Hantek 365 software. The 280-nm absorbance wavelength is commonly used for chromatographic protein measurements (66). Solutions of 70 μM transferrin (>98%; Sigma) with varied ionic concentrations are prepared in 10 mM Hepes buffer (pH 7.2; Sigma). Approximately 300 µL of each solution tested is injected into the FPLC system. All separations are performed at an average flow rate of 1.7 mL/min. The salt concentration of the feed Hepes buffer is identical to each tested condition, ensuring the salt concentration of the injection solution matched the salt concentration of the feed solution. For all separations, a series of 4 nylon 6,6 membrane filters (25-mm diameter, 21 mm thick, 3.9-cm² filtration area, nonsterile: Biomed Scientific) are connected in series to the FPLC setup. Surface identity of nylon 6,6 membranes and nylon 6,6 used in single-molecule experiments is confirmed to be chemically identical with X-ray photoelectron spectroscopy (SI Appendix, Fig. S3). A series of membrane filters is chosen given recent commonplace in downstream separations (62, 67).

Monte Carlo Chromatographic Simulations. Simulated chromatograms using kinetics extracted from single-molecule tracking experiments are performed using custom Python scripts based on the mathematical construction of Giddings and Eyring (68). The elution time of a single molecule is $T = t_m + \sum_{i=1}^{m} \tau_{i,j}$, where T is the total elution time, t_m is the amount of time spent in the mobile phase, and $\tau_{i,i}$ is the desorption time of the i^{th} desorption event via the ith desorption pathway. Simulation sets are initialized to contain 2 desorption pathways (m=2), adopting the calculated desorption rate and prevalence of each desorption pathway from single-molecule kinetics. Elution is simulated by assuming 500,000 molecules all migrate down a column with 100 possible adsorption events, averaging 50 adsorption events per molecule. Desorption times from each event are summed together with a constant mobile phase time $\left(t_{m}\right)$ to calculate the retention time of each molecule. Simulated chromatograms are then created by binning the molecule retention times to the time resolution of the simulated clock. All scripts used to run the simulations are available for download at https://github.com/LandesLab?tab=repositories.

Processing of Simulated Chromatograms. Statistical information is drawn from the raw molecule counts before any data processing. Simulated chromatographic curves are smoothed using a Savitzky–Golay filter (69) as provided by the Python SciPy package. The smoothed data are then fit using a cubic spline to transition the curve shape to a polynomial form. All data presented

in figures are available in an online directory at https://rice.box.com/s/ n3cmfg5ji0lmw4fxt5gsqnzxho5rxfy1.

Results and Discussion

Transferrin Surface Dynamics. Single-molecule tracking resolves 2 distinct modes of transferrin surface dynamics at nylon, which are tuned by salt concentration. One population exhibits a continuous-time random walk (CTRW) on nylon while the second population undergoes single-site adsorption-desorption (Fig. 1 A-C). Proteins exhibiting a CTRW display periods of immobile physisorption disrupted by surface exploration to nearby adsorption sites (70). CTRWs, present in transferrin–nylon interactions, can be identified by waiting time distributions that fit a power law (SI Appendix, Fig. S4) (71, 72). The prevalence of transferrin molecules undergoing CTRWs decreased as salt concentration increased, resulting in more single-site adsorption-desorption. However, CTRWs remained the dominant mode of transferrin surface transport (Fig. 1 A-C). Representative single-molecule trajectories at varied ionic conditions in Fig. 1B illustrate the 2 modes of dynamics that transferrin displays at nylon. The dynamics are spatially resolved below the diffraction limit of light (39, 73). Spatial trajectory filtering is applied to quantify and classify dynamics as either CTRW (Fig. 1B, cyan) or single-site adsorption-desorption (Fig. 1B, magenta). In short, if a transferrin molecule moved >22 nm from the initial localization position during a trajectory, a length scale greater than our localization precision, the trajectory is classified as CTRW (details in SI Ap-

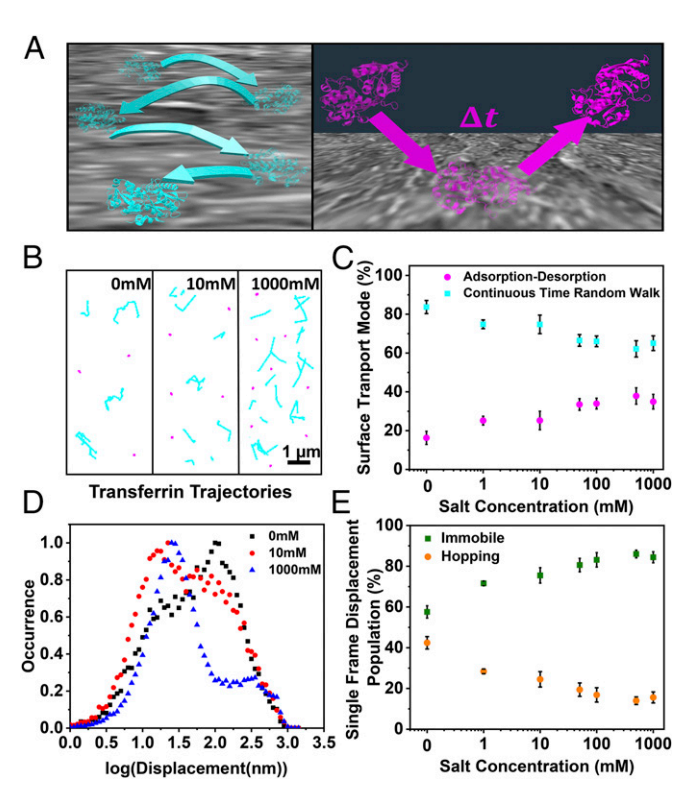


Fig. 1. Transferrin surface dynamics at nylon at varied ionic strengths. (A) Cartoon representation of 2 modes of transferrin-nylon interaction, CTRW (cyan) and single-site adsorption-desorption (magenta) [Protein Data Bank (PDB) ID code 1D3K (74)]. (B) Representative single-molecule transferrin trajectories at nylon interface undergoing a CTRW (cyan) and single-site adsorption-desorption (magenta). (C) Percentage of transferrin molecules exhibiting CTRW vs. simple adsorption-desorption. (D) Single-frame displacement distributions at varied ionic strengths. (E) Percent of single frame displacements contributing to immobile and hopping surface transport from sampling distributions in C. The 0 mM condition is shown on logarithmic scale in C and E in order to display the entire range of salt concentrations.

pendix) (37, 65). The relative percentage of the 2 populations as a function of salt is shown in Fig. 1C. Tracking results show that increased salt concentrations resulted in a relative decrease of $18 \pm 3\%$ in CTRW of transferrin at nylon. Although the transition to pure adsorption-desorption is not complete, the observed saltdependent changes in surface dynamics hold important implications for the ensemble elutions and simulations presented later. Transferrin surface diffusion is non-Brownian, and diffusion coefficient values are calculated and compared with bulk diffusion measurements (SI Appendix, Table S1). Additional mechanistic details are also revealed by analyzing frame-to-frame displacements, discussed next.

Single-frame displacement distributions quantify the shift toward immobile adsorption events at high salt concentrations (Fig. 1D). Two spatially resolvable populations of displacements have been reported before in dye-multilayer polyelectrolyte interactions (47) but never in the case of protein-polymer interactions to our knowledge. Single-frame displacement distributions are histograms quantifying the distance a molecule travels frame to frame. It must be noted that a single protein trajectory can contribute to both populations observed in Fig. 1D if a molecule experiences periods of confinement and hopping. A previously published Markov chain Monte Carlo (MCMC) algorithm quantifies both the relative percentage and the mean hop distance of the 2 distinct populations in the single-frame displacement distributions (Fig. 1D and SI Appendix, Fig. S5) (47). The MCMC algorithm removes any statistical bias attributed to selected distribution bin sizes by generating distributions that model the experimental data (47). Analysis of the single-frame displacements indicates that a 27 \pm 3% decrease in frame-to-frame hopping is observed as salt concentrations are increased from 0 mM to 1000 mM in a tunable fashion (Fig. 1 D and E). Displacement distribution results are independent of the order in which salt is introduced, indicating transferrin transport is reversible under the steady-state flow conditions used here (SI Appendix, Fig. S6). Single-frame displacement analyses indicate that after the initial adsorption of a transferrin molecule the likelihood of transferrin exploring nearby sites is decreased at high salt concentrations. The combination of trajectory spatial filtering and single-frame displacement distribution analyses reveal that as salt concentration is increased single-site adsorption-desorption behavior of transferrin increases, accompanied by a lower probability of surface exploration. Single-molecule tracking lends mechanistic insight into the multifaceted surface transport of transferrin at nylon and also quantifies kinetic changes in transferrin-nylon interactions.

Single-Molecule Transferrin Kinetics. Transferrin adsorption rates increase on the nylon interface at higher salt concentrations, reaching roughly a 10-fold increase at a salt concentration of 500 mM (Fig. 24). The rate of adsorption is quantified by counting the number of new identified molecules that arrive at the interface per unit area and time. Increases in adsorption rates at increased ionic strengths correlate to more transferrin molecules imaged at the surface (Fig. 24). Quantifying the absolute adsorption rates is often experimentally unachievable but can easily be achieved with single-molecule tracking (75, 76). One explanation for the increased binding at higher salt concentration is a decreased solubility of transferrin molecules in the mobile phase as predicted by Hofmeister (19, 77), but this explanation is debated to date (78, 79). Similar increased adsorption kinetics observed with Hofmeister salts at the single-molecule level predicted that increased hydrophobic interactions lead to higher rates of adsorption (75). Another possible driving force in transferrin–nylon interactions is the electrostatic screening of repulsive interactions between transferrin (pI 5.6) (80) and nylon (zeta potential -21 ± 1 mV), both of which carry a negative charge at pH 7.2 (81-83). Electrostatic forces dominating the adsorption rate changes of proteins at interfaces have been explored by Schwartz and

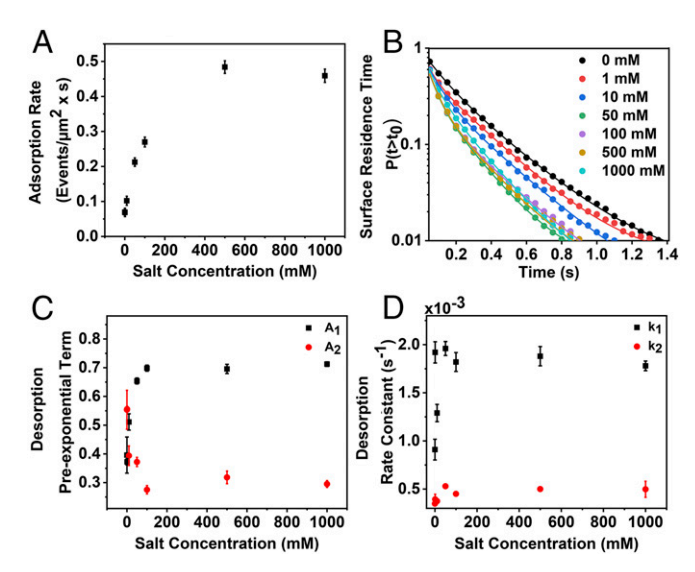


Fig. 2. Transferrin kinetics at nylon at varied ionic strengths. (*A*) Rate of adsorption. (*B*) Surface residence time distributions represented in a cumulative distribution and fit to a double exponential decay with solid lines (Eq. 1). (*C*) Preexponential coefficients from fitting results in *B*. (*D*) Desorption rate constants from fits in plot (*B*).

coworkers in addition to short-range interactions dictating desorption kinetics (76). Increased adsorption rates indicate that the transferrin molecules exhibit a greater attraction for the nylon interface as salt is increased in the mobile phase. In addition to adsorption kinetics, single-molecule results also elucidate desorption kinetics of transferrin, as discussed next.

Surface residence time analyses uncover 2 distinct populations of transferrin desorption from the nylon interface, revealing an overall increase in desorption rates accompanied by a decrease in rare long-lived events. Surface residence time distributions (Fig. 2B) are represented as cumulative distribution functions (CDF) to uncover rare long-lived binding events (84), which have a large influence on protein separation efficiencies as discussed in later sections (24, 68, 85). Surface residence time distributions are fit to a 2-term exponential decay,

$$P(t) = A_1 e^{-k_1 t} + A_2 e^{-k_2 t},$$
 [1]

to identify the desorption kinetics of transferrin molecules. Exponential decays are used to quantify single-molecule interfacial desorption kinetics from surface residence time distributions (52). CDF plots are shown for all salt conditions tested with corresponding fits to Eq. 1 in Fig. 2B. Visual inspection of the tails of CDF distributions highlights that increasing salt concentration decreases the number of rare long-lived adsorption events at nylon (Fig. 2B). CDF fitting is used to calculate the respective prevalence (Fig. 2C) and desorption rate constants for the 2 individual populations of surface-residing transferrin molecules (Fig. 2D). The dominant desorption pathway of transferrin is changed at salt concentrations greater than 10 mM (Fig. 2C). Desorption is dominated by fast dynamics at salt concentrations greater than 10 mM, in comparison to slow kinetics in the lower- and no-salt conditions (Fig. 2C). Spatial filtering described above is applied to show the fast desorption population is dominated by molecules undergoing single-site adsorptiondesorption given they desorb quicker from nylon in comparison to transferrin molecules undergoing a CTRW (SI Appendix, Table S2). We believe that the slow desorption component in our kinetic analysis most likely represents the CTRW fraction, supported by the strong correlation (r = 0.91) between the decrease in A_2 (Fig.

2C) and the decrease in CTRW (Fig. 1C). CDF fit results show the desorption rate constant (k_1) for the fast population increased as a function of salt, whereas the slow population desorption rate constant (k_2) is unchanged, leading to an overall increase in desorption (Fig. 2D). The conformational stability of transferrin is quantified with a denaturation experiment (SI Appendix, Fig. S7), showing that conformation is more robust with increased salt concentration. Stability increases could contribute to increased desorption rates observed from nylon at higher salt conditions. These results highlight the utility of single-molecule techniques to quantify kinetic metrics in highly dynamic and complex chromatographic systems (86–88).

Ensemble CD. Transferrin adsorption to the nylon interface induces the partial unfolding of transferrin, which is enhanced at higher ionic strengths (Fig. 3 *A*–*C*). CD spectroscopy is utilized to interrogate the secondary structural motifs that are present in a protein's structure (89). CD results show that a reduction in the alpha-helical secondary structure is observed for adsorbed transferrin molecules on nylon microspheres, suggesting that transferrin adopts a partially unfolded conformation at nylon interfaces in the absence of salt (Fig. 3*C*, blue). A further reduction in alpha-helical structure is observed in a tunable fashion with increased salt concentrations (Fig. 3*C*). This transferrin unfolding appears to be a surface-induced phenomenon as unfolding is only observed in

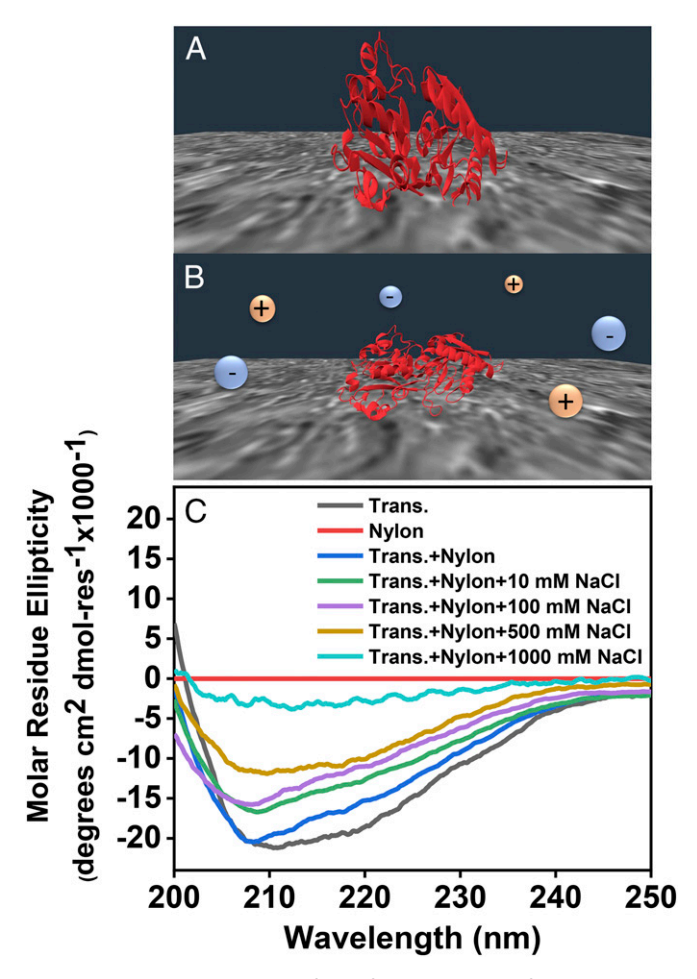
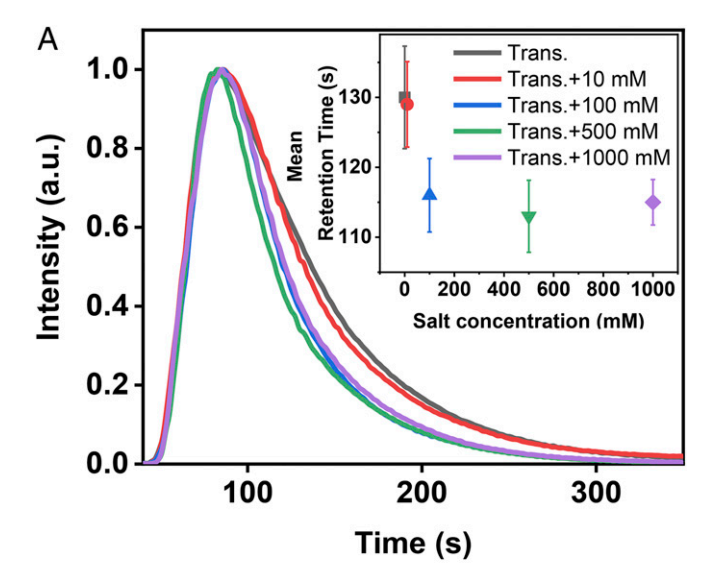


Fig. 3. Structural examination of transferrin at nylon surface under varied ionic conditions. Cartoon depiction of folded transferrin (A) and unfolded transferrin (B) at nylon in the presence of salt [PBD ID code 1D3K (74)]. (C) Ensemble CD spectroscopy of transferrin at varied ionic conditions in the presence of nylon microspheres.

the presence of nylon microspheres and is not induced by salt alone (SI Appendix, Fig. S8). Surface-induced unfolding of proteins and a resulting change in transport dynamics has been observed at the single-molecule level by others (72, 90). Surface-induced structural changes would not alter adsorption kinetics under our conditions (Fig. 24) since unfolding is a surface-induced effect. However, structural changes of transferrin likely play a dominant role in the observed varied surface transport modes (Fig. 1) and surface desorption kinetics (Fig. 2 B-D), given the large CD signal modulation as salt conditions are tuned. We predict and confirm that single-site adsorption-desorption at nylon is dominated by unfolded transferrin molecules by quantifying surface dynamics of chemically unfolded transferrin molecules (SI Appendix, Fig. S9). We also confirm that the unfolded structure of transferrin contributes to the increased desorption rates observed at high salt concentrations with the observed desorption kinetics from chemically unfolded transferrin molecules (SI Appendix, Fig. S10). Waiting time analyses, which quantify the time spent per site, confirm that although overall transferrin desorption rates increase with increased salt (Fig. 2) the time spent per site increases (SI Appendix, Fig. S11) but at fewer sites (Fig. 1 D and E). Increased residence times once a protein unfolds on a surface has been well studied by others (72). Salt-induced structural changes to nylon are ruled out as a major contributor to our observed transferrin dynamics because the timescale on which salt alters nylon hydration occurs over hours (91). Therefore, transferrin unfolding has a direct effect on the surface transport dynamics both spatially and kinetically under salting out conditions. CD results conducted with rhodamine B-labeled transferrin used in single-molecule experiments that confirm the addition of rhodamine labels does not alter transferrin interactions with nylon (SI Appendix, Fig. S12).

FPLC. We suggest that increased transferrin desorption kinetics and transferrin conformational changes upon adsorption presented above provide a mechanistic explanation for the utility of salting out in protein elutions (Fig. 4). Ensemble FPLC of transferrin on nylon 6,6 membranes at increasing salt concentrations exhibits peak narrowing (Fig. 4A). The decrease in broadening is illustrated in Fig. 4B with the full width half maximum (FWHM) of the chromatograms, which is one way to compare peak widths in chromatographic studies (92). The decrease in mean retention time observed (Fig. 4 A, Inset) aligns with the increased desorption kinetics observed at the single-molecule level (Fig. 2 B-D). Constant salt concentrations are used here because a single type of protein is being purified (93), in contrast to salt gradients, which are required for separating mixtures of proteins. It is important to note that constant salt concentrations are also used for discovering the appropriate concentrations for separating individual analytes from a mixture when a salt gradient is employed (94). Overcrowding effects at nylon membranes are ruled out by separations performed with lower transferrin concentrations one order of magnitude above our detection limit (7 μM). Similar line shapes and peak narrowing effects are observed at lower concentrations independent of the order of salt concentrations tested (SI Appendix, Fig. S13). Similar line shapes and fewer filters have been utilized by others performing protein FPLC, further ruling out overcrowding effects (95, 96). The interaction of transferrin with nylon membranes is confirmed with CD measurements of an eluted fraction of transferrin at high salt (SI Appendix, Fig. S14).

Importantly, the mechanistic link between the single-protein kinetics presented in Fig. 2B and peak width is provided in Giddings' and Eyring's statistical theory of chromatography (24). In the present work, increased desorption kinetic rates are observed at the single-molecule level in addition to the suppression of long-lived binding events dominated by the CTRW surface transport (Fig. 2 and SI Appendix, Table S2). We predict that the suppression of CTRW lowered the probability of long-lived events, leading to profile narrowing (Fig. 4). This can be intuitively understood



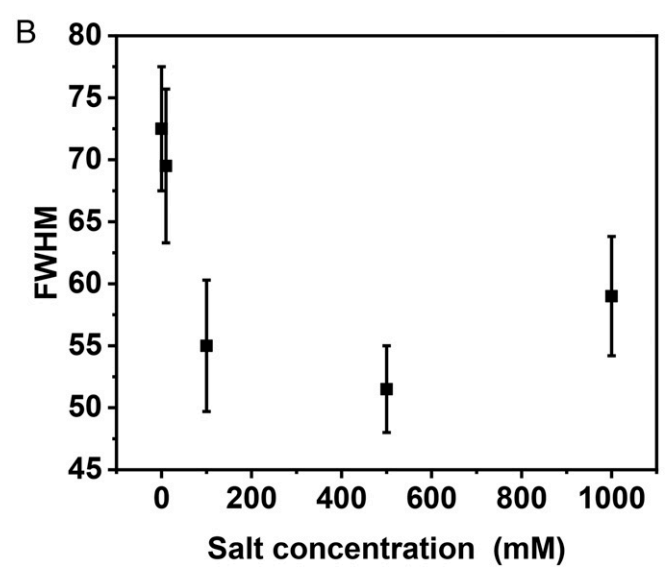


Fig. 4. FPLC of transferrin with nylon membranes. (A) Transferrin chromatograms under salting out conditions with calculated mean retention times and standard deviation from triplicate separations (*Inset*). (B) FWHM of chromatograms shown in A.

in the context of work by Schwartz and coworkers where a molecule exhibiting a CTRW will increase the probability of interacting with anomalously strong adsorption sites, thereby increasing the prevalence of long-lived events (97). The observation of increased desorption kinetics reducing chromatographic tailing in liquid-based separations has been reported by others (85). An overall decrease in the mean retention time of transferrin with increasing salt (Fig. 4 A, Inset), accompanied with increased desorption rates observed at the single-molecule level (Fig. 2), gives a microscopic explanation for macroscale separations with salting-out conditions, in which the analyte elutes more quickly with the addition of salt (98). Monte Carlo simulations based on single-molecule kinetics further support the conclusion of reduced broadening.

Monte Carlo Chromatographic Simulations. Monte Carlo simulations underpinned by the stochastic theory of Giddings and Eyring (68) reveal that the kinetic data extracted from surface residence time fits (Fig. 2B) predicts better-resolved chromatographic peaks as salt increases. Simulated chromatograms are

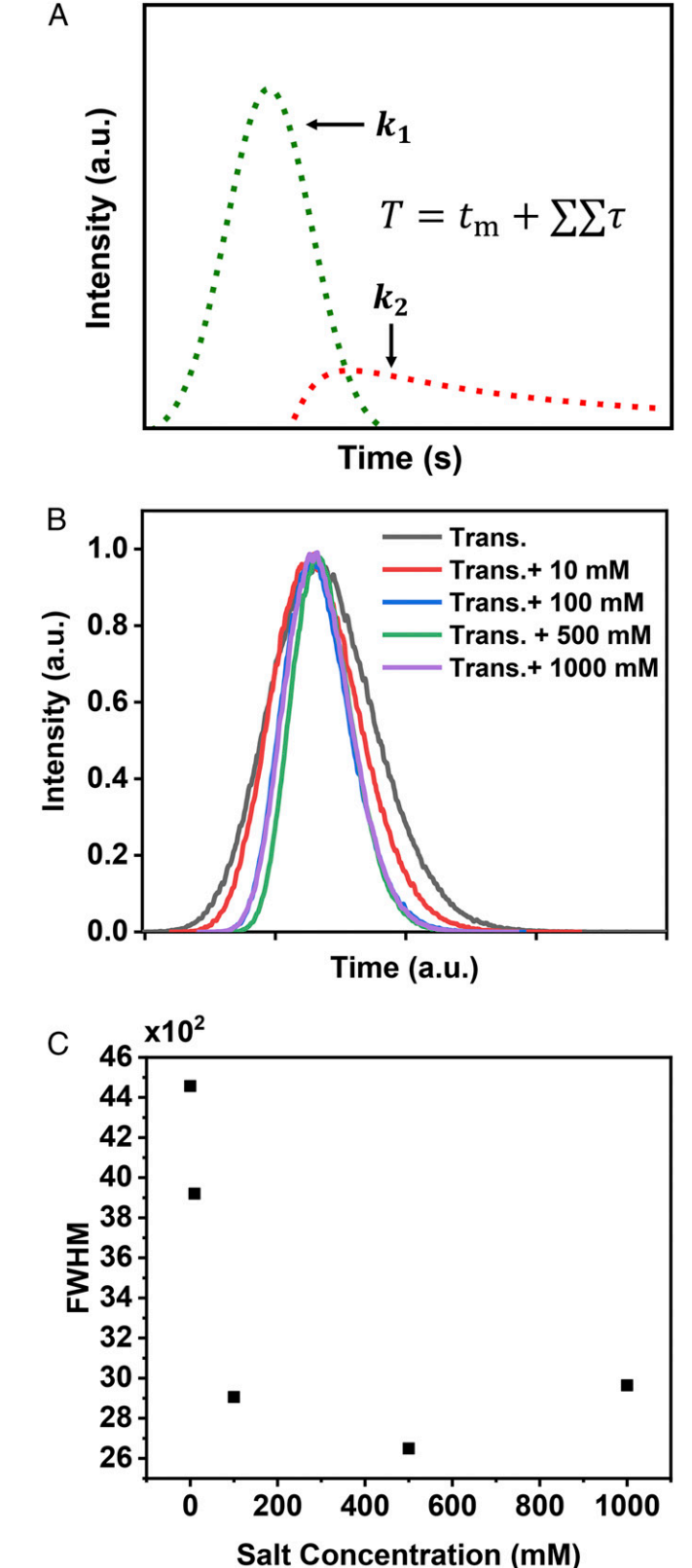


Fig. 5. Simulated chromatograms using Monte Carlo simulations. (*A*) Cartoon depicting contribution of 2 desorption rate constants on final elution profile line shape. (*B*) Peak aligned chromatograms simulated from 500,000 molecules using values extracted from CDF fits shown in Fig. 2 B–D. (*C*) Measured FWHM of the peaks shown in B.

generated using the preexponential coefficients (Fig. 2C) and desorption rate constants (Fig. 2D) found from the experimental fits of the surface residence time (Fig. 5A). Similar methods were employed by Dondi et al. (99) and Cavazzini et al. (100) to explore the effects of limited site availability as well as illustrate the equivalence of the stochastic theory and the macroscopic lumped kinetic model. Increases in salt show a qualitative thinning of the profile and a visual decrease in the formation of a chromatographic tail (Fig. 5B). Measurements of the FWHM of corresponding peaks support the conclusion that increasing the salt concentration of the mobile phase increases chromatographic efficiency via profile thinning (Fig. 5C). Symmetric broadening/ thinning is a direct result of the number of interactions that a protein has with the stationary phase surface. We deduce that profile thinning is driven by the reduction of CTRWs within the protein history, an effect that corroborates Giddings' theories (101). Simulations and experimental evidence corroborate previous studies showing that a decrease in long-lived adsorption events (16) observed here through increased salt content produce narrower, more symmetric chromatographic peaks (24, 102). The physical origin of the altered kinetics here is revealed in the single-molecule results which indicate that a decrease in CTRW dynamics (Fig. 1 A-C) at nylon decreases the prevalence of rare long-lived adsorption events (Fig. 2B). The change in observed surface dynamics is facilitated by structural changes induced to transferrin at nylon (Fig. 3 and SI Appendix, Fig. S8). The combination of our simulations and singlemolecule results indicate that mobile-phase effects are major contributors to peak symmetry. Other groups identified how heterogeneous mobile-phase mixing among the components of the chromatographic column introduces asymmetry/broadening (103, 104). Examples of mobile-phase effects include turbulent flow occurring at column junctions, including the injection port, column connection, and detector port, which can introduce profile broadening that varies between instru-

Our simulations illustrate broadening produced by our measured kinetic differences isolated from mobile-phase effects. Experimental FPLC measurements (Fig. 4) provide a convolution of both kinetic and mobile-phase contributions to peak shape that cannot be separated empirically (105). By peak aligning, we remove elution contributions from the mobile-phase time and varied retention times to emphasize the broadening effects predicted by desorption kinetics. Exclusion of other effects from the mobile phase guarantees that changes in the chromatographic shape arise from kinetic differences alone. Future advancements in the Monte Carlo model, as well as single-molecule tracking, will aid in deconvoluting instrumental contributions from chemical effects.

Conclusion

Single-molecule surface transport modes and kinetic analyses coupled with ensemble CD have guided a mechanistic explanation for increased separation efficiency observed in bulk separations during the salting-out process. Predicting peak broadening from single-molecule kinetics is further supported by simulation of elution profiles. The increasing prevalence of single-site adsorption-desorption of transferrin at nylon is directly modulated with salt concentration (Fig. 1). Increasing salt concentration led to an increase in adsorption and desorption kinetics at the nylon stationary phase (Fig. 2). Electrostatic shielding likely dominates the adsorption rate increase, while the increased overall rate of desorption and increased waiting times are attributed to surface-induced structural changes to transferrin at higher salt concentrations (Fig. 3 and SI Appendix, Figs. S8-S10). Altered desorption kinetics from salting were not observed with fatty acid probe molecules (75), highlighting the complexity of large

biomolecules that exhibit complicated dynamics such as unfolding. The reduction in chromatographic broadening found in ensemble separations of transferrin (Fig. 4) is explained by a decrease in rare long-lived binding (Fig. 2B) that correlates to a decrease in the CTRW motion (Fig. 1). The utility of singlemolecule tracking to mechanistically explain ensemble chromatographic observables is highlighted in our work. Further, our findings emphasize the importance of understanding the physiochemical changes salting-out processes can have on protein behavior in bench-top and industrial-scale separations. The

- 1. J. Avorn, The \$2.6 billion pill-Methodologic and policy considerations. N. Engl. J. Med. 372, 1877-1879 (2015).
- 2. S. Ahuja, Handbook of Bioseparations (Academic Press, 2000).
- 3. E. S. Langer, Annual report and survey of biopharmaceutical manufacturing capacity and production (BioPlan Associates, 2017).
- 4. Q. Lan, A. S. Bassi, J.-X. Zhu, A. Margaritis, A modified Langmuir model for the prediction of the effects of ionic strength on the equilibrium characteristics of protein adsorption onto ion exchange/affinity adsorbents. Chem. Eng. J. 81, 179-186
- 5. T. Burnouf, M. Radosevich, Affinity chromatography in the industrial purification of plasma proteins for therapeutic use. J. Biochem. Biophys. Methods 49, 575-586 (2001).
- 6. A. Ladiwala, K. Rege, C. M. Breneman, S. M. Cramer, A priori prediction of adsorption isotherm parameters and chromatographic behavior in ion-exchange systems. Proc. Natl. Acad. Sci. U.S.A. 102, 11710-11715 (2005).
- 7. E. J. Castillo, J. L. Koenig, J. M. Anderson, J. Lo, Characterization of protein adsorption on soft contact lenses. I. Conformational changes of adsorbed human serum albumin. Biomaterials 5, 319-325 (1984).
- 8. N. B. Omali, L. N. Subbaraman, C. Coles-Brennan, Z. Fadli, L. W. Jones, Biological and clinical implications of lysozyme deposition on soft contact lenses. Optom. Vis. Sci. 92, 750-757 (2015).
- 9. J. I. Hahm, Fundamentals of nanoscale polymer-protein interactions and potential contributions to solid-state nanobioarrays. Langmuir 30, 9891-9904 (2014).
- 10. J. I. Hahm, Functional polymers in protein detection platforms: Optical, electrochemical, electrical, mass-sensitive, and magnetic biosensors. Sensors (Basel) 11, 3327-3355 (2011).
- 11. M. Chen, S. Khalid, M. S. Sansom, H. Bayley, Outer membrane protein G: Engineering a quiet pore for biosensing. Proc. Natl. Acad. Sci. U.S.A. 105, 6272-6277 (2008).
- 12. S. E. Baker, P. E. Colavita, K.-Y. Tse, R. J. Hamers, Functionalized vertically aligned carbon nanofibers as scaffolds for immobilization and electrochemical detection of redox-active proteins. Chem. Mater. 18, 4415-4422 (2006).
- 13. T. L. Clare, B. H. Clare, B. M. Nichols, N. L. Abbott, R. J. Hamers, Functional monolayers for improved resistance to protein adsorption: Oligo(ethylene glycol)modified silicon and diamond surfaces. Langmuir 21, 6344-6355 (2005).
- 14. R. N. Sargent, D. L. Graham, Salting-out chromatography of serum proteins. Anal. Chim. Acta 30, 101-104 (1964).
- T. Arakawa, S. N. Timasheff, Mechanism of protein salting in and salting out by divalent cation salts: Balance between hydration and salt binding. Biochemistry 23, 5912-5923 (1984).
- 16. L. Kisley et al., High ionic strength narrows the population of sites participating in protein ion-exchange adsorption: A single-molecule study. J. Chromatogr. A 1343, 135-142 (2014).
- 17. M. C. Stone, Y. Tao, G. Carta, Protein adsorption and transport in agarose and dextran-grafted agarose media for ion exchange chromatography: Effect of ionic strength and protein characteristics. J. Chromatogr. A 1216, 4465-4474 (2009).
- 18. H. I. Okur et al., Beyond the Hofmeister series: Ion-specific effects on proteins and their biological functions. J. Phys. Chem. B 121, 1997-2014 (2017).
- 19. F. Hofmeister, Zur Lehre von der Wirkung der Salze–Untersuchungen über den Quellungsvorgang. Archiv für experimentelle Pathologie und Pharmakologie 27,
- 20. Y. Zhang, P. S. Cremer, The inverse and direct Hofmeister series for lysozyme. Proc. Natl. Acad. Sci. U.S.A. 106, 15249-15253 (2009).
- 21. K. Tsumoto, D. Ejima, A. M. Senczuk, Y. Kita, T. Arakawa, Effects of salts on proteinsurface interactions: Applications for column chromatography. J. Pharm. Sci. 96, 1677-1690 (2007).
- 22. A. Saxena, B. P. Tripathi, M. Kumar, V. K. Shahi, Membrane-based techniques for the separation and purification of proteins: An overview. Adv. Colloid Interface Sci. 145, 1-22 (2009)
- 23. S. R. Dziennik et al., Nondiffusive mechanisms enhance protein uptake rates in ion exchange particles. Proc. Natl. Acad. Sci. U.S.A. 100, 420-425 (2003).
- 24. J. C. Giddings, Kinetic origin of tailing in chromatography. Anal. Chem. 35, 1999-2002 (1963).
- 25. National Academies of Sciences Engineering, and Medicine, A Research Agenda for Transforming Separation Science (National Academy of Sciences, Washington, DC,
- 26. H. Vaisocherová et al., Ultralow fouling and functionalizable surface chemistry based on a zwitterionic polymer enabling sensitive and specific protein detection in undiluted blood plasma. Anal. Chem. 80, 7894-7901 (2008).
- 27. N. Welsch, Y. Lu, J. Dzubiella, M. Ballauff, Adsorption of proteins to functional polymeric nanoparticles. Polymer 54, 2835-2849 (2013).

design of stationary phase supports that suppress anomalous CTRW diffusion at the stationary phase will lead to improved separation efficiencies.

ACKNOWLEDGMENTS. C.F.L. acknowledges the Welch Foundation (Grant C-1787) and the National Science Foundation (CHE-1808382) for support of this work. We thank Stephan Link and his group (Welch C-1664). N.A.M., N.C.C., and L.D.C.B. acknowledge that this material is based upon work supported by the National Science Foundation Graduate Research Fellowship Program (Grant 1842494). We also thank Dr. Chayan Dutta for scientific

- 28. F. Rico, A. Russek, L. González, H. Grubmüller, S. Scheuring, Heterogeneous and ratedependent streptavidin-biotin unbinding revealed by high-speed force spectroscopy and atomistic simulations. Proc. Natl. Acad. Sci. U.S.A. 116, 6594-6601 (2019).
- 29. H. Shen et al., Single particle tracking: From theory to biophysical applications. Chem. Rev. 117, 7331-7376 (2017).
- 30. W. Wang et al., Super temporal-resolved microscopy (STReM). J. Phys. Chem. Lett. 7, 4524-4529 (2016)
- 31. J. Deich, E. M. Judd, H. H. McAdams, W. E. Moerner, Visualization of the movement of single histidine kinase molecules in live Caulobacter cells. Proc. Natl. Acad. Sci. U.S.A. 101, 15921-15926 (2004).
- 32. A. E. Cohen, W. E. Moerner, Suppressing Brownian motion of individual biomolecules in solution. Proc. Natl. Acad. Sci. U.S.A. 103, 4362-4365 (2006).
- 33. J. Wiedenmann et al., EosFP, a fluorescent marker protein with UV-inducible greento-red fluorescence conversion. Proc. Natl. Acad. Sci. U.S.A. 101, 15905-15910 (2004).
- 34. A. D. Radadia et al., Control of nanoscale environment to improve stability of immobilized proteins on diamond surfaces. Adv. Funct. Mater. 21, 1040-1050 (2011).
- 35. W. K. Chung, A. S. Freed, M. A. Holstein, S. A. McCallum, S. M. Cramer, Evaluation of protein adsorption and preferred binding regions in multimodal chromatography using NMR. Proc. Natl. Acad. Sci. U.S.A. 107, 16811-16816 (2010).
- 36. E. M. Peterson, M. W. Manhart, J. M. Harris, Single-molecule fluorescence imaging of interfacial DNA hybridization kinetics at selective capture surfaces. Anal. Chem. 88, 1345-1354 (2016).
- 37. H. Shen et al., Single-molecule kinetics of protein adsorption on thin nylon-6,6 films. Anal. Chem. 88, 9926-9933 (2016).
- 38. B. Shuang et al., Generalized recovery algorithm for 3D super-resolution microscopy using rotating point spread functions. Sci. Rep. 6, 30826 (2016).
- 39. B. Shuang, J. Chen, L. Kisley, C. F. Landes, Troika of single particle tracking programing: SNR enhancement, particle identification, and mapping. Phys. Chem. Chem. Phys. 16, 624-634 (2014).
- 40. W. Wang et al., Super-temporal resolved microscopy reveals multistep desorption kinetics of α-lactalbumin from nylon. Langmuir 34, 6697-6702 (2018).
- 41. Y. Shechtman, L. E. Weiss, A. S. Backer, S. J. Sahl, W. E. Moerner, Precise threedimensional scan-free multiple-particle tracking over large axial ranges with tetrapod point spread functions, Nano Lett. 15, 4194-4199 (2015).
- 42. S. Quirin, S. R. P. Pavani, R. Piestun, Optimal 3D single-molecule localization for superresolution microscopy with aberrations and engineered point spread functions. Proc. Natl. Acad. Sci. U.S.A. 109, 675-679 (2012).
- 43. W. Wang et al., Generalized method to design phase masks for 3D super-resolution microscopy. Opt. Express 27, 3799-3816 (2019).
- 44. L. Kisley et al., Competitive multicomponent anion exchange adsorption of proteins at the single molecule level. Analyst 142, 3127-3131 (2017).
- 45. L. J. Tauzin et al., Variable surface transport modalities on functionalized nylon films revealed with single molecule spectroscopy. RSC Adv. 6, 27760-27766 (2016).
- 46. N. A. Moringo et al., Variable lysozyme transport dynamics on oxidatively functionalized polystyrene films. Langmuir 33, 10818-10828 (2017).
- 47. L. J. Tauzin et al., Charge-dependent transport switching of single molecular ions in a weak polyelectrolyte multilayer. Langmuir 30, 8391-8399 (2014).
- 48. M. J. Wirth, D. J. Swinton, Single-molecule probing of mixed-mode adsorption at a chromatographic interface. Anal. Chem. 70, 5264-5271 (1998).
- 49. H. Shen, W. Xu, P. Chen, Single-molecule nanoscale electrocatalysis. Phys. Chem. Chem. Phys. 12, 6555-6563 (2010).
- 50. H. Shen, X. Zhou, N. Zou, P. Chen, Single-molecule kinetics reveals a hidden surface reaction intermediate in single-nanoparticle catalysis. J. Phys. Chem. C 118, 26902-26911 (2014)
- 51. N. M. Andoy et al., Single-molecule catalysis mapping quantifies site-specific activity and uncovers radial activity gradient on single 2D nanocrystals. J. Am. Chem. Soc. 135. 1845-1852 (2013).
- 52. E. M. Peterson, M. W. Manhart, J. M. Harris, Competitive assays of label-free DNA hybridization with single-molecule fluorescence imaging detection. Anal. Chem. 88, 6410-6417 (2016).
- 53. E. M. Peterson, M. W. Manhart, D. M. Kriech, J. M. Harris, "Fluorescence microscopy of single-molecule DNA hybridization at high density interfaces" in Abstracts of Papers of the American Chemical Society (ACS, 2014), p. 248
- 54. M. Schickinger, M. Zacharias, H. Dietz, Tethered multifluorophore motion reveals equilibrium transition kinetics of single DNA double helices. Proc. Natl. Acad. Sci. U.S.A. 115, E7512-E7521 (2018).
- 55. L. E. Weiss, L. Milenkovic, J. Yoon, T. Stearns, W. E. Moerner, Motional dynamics of single Patched1 molecules in cilia are controlled by Hedgehog and cholesterol. Proc. Natl. Acad. Sci. U.S.A. 116, 5550-5557 (2019)

- C. Yu, S. Granick, Revisiting polymer surface diffusion in the extreme case of strong adsorption. *Langmuir* 30, 14538–14544 (2014).
- S. A. Sukhishvili, S. Granick, Adsorption of human serum albumin: Dependence on molecular architecture of the oppositely charged surface. J. Chem. Phys. 110, 10153– 10161 (1999).
- T. R. Daniels et al., The transferrin receptor and the targeted delivery of therapeutic agents against cancer. Biochim. Biophys. Acta 1820, 291–317 (2012).
- W. Liang, Q. Li, N. Ferrara, Metastatic growth instructed by neutrophil-derived transferrin. Proc. Natl. Acad. Sci. U.S.A. 115, 11060–11065 (2018).
- P. Jain, M. K. Vyas, J. H. Geiger, G. L. Baker, M. L. Bruening, Protein purification with polymeric affinity membranes containing functionalized poly(acid) brushes. *Bio-macromolecules* 11, 1019–1026 (2010).
- 61. X. Zeng, E. Ruckenstein, Membrane chromatography: Preparation and applications to protein separation. *Biotechnol. Prog.* **15**, 1003–1019 (1999).
- V. Orr, L. Zhong, M. Moo-Young, C. P. Chou, Recent advances in bioprocessing application of membrane chromatography. *Biotechnol. Adv.* 31, 450–465 (2013).
- I. Kolesov, D. Mileva, R. Androsch, Mechanical behavior and optical transparency of polyamide 6 of different morphology formed by variation of the pathway of crystallization. *Polym. Bull.* 71, 581–593 (2014).
- S. Handley, Nylon: The Story of a Fashion Revolution: A Celebration of Design from Art Silk to Nylon and Thinking Fibres (Johns Hopkins University Press, 1999).
- L. Kisley et al., Unified superresolution experiments and stochastic theory provide mechanistic insight into protein ion-exchange adsorptive separations. Proc. Natl. Acad. Sci. U.S.A. 111, 2075–2080 (2014).
- D. V. Camper, R. E. Viola, Fully automated protein purification. Anal. Biochem. 393, 176–181 (2009).
- S.-Y. Suen, Y.-C. Liu, C.-S. Chang, Exploiting immobilized metal affinity membranes for the isolation or purification of therapeutically relevant species. J. Chromatogr. B Analyt. Technol. Biomed. Life Sci. 797, 305–319 (2003).
- J. C. Giddings, H. Eyring, A molecular dynamic theory of chromatography. J. Phys. Chem. 59, 416–421 (1955).
- A. Savitzky, M. J. Golay, Smoothing and differentiation of data by simplified least squares procedures. Anal. Chem. 36, 1627–1639 (1964).
- D. Wang, H.-Y. Chin, C. He, M. P. Stoykovich, D. K. Schwartz, Polymer surface transport is a combination of in-plane diffusion and desorption-mediated flights. ACS Macro Lett. 5, 509–514 (2016).
- M. J. Skaug, J. Mabry, D. K. Schwartz, Intermittent molecular hopping at the solidliquid interface. *Phys. Rev. Lett.* 110, 256101 (2013).
- J. S. Weltz, D. K. Schwartz, J. L. Kaar, Surface-mediated protein unfolding as a search process for denaturing sites. ACS Nano 10, 730–738 (2016).
- B. Shuang et al., Improved analysis for determining diffusion coefficients from short, single-molecule trajectories with photoblinking. Langmuir 29, 228–234 (2013).
- A. H.-W. Yang et al., Crystal structures of two mutants (K206Q, H207E) of the N-lobe of human transferrin with increased affinity for iron. Protein Sci. 9, 49–52 (2000).
- N. Nelson, D. K. Schwartz, Specific ion (Hofmeister) effects on adsorption, desorption, and diffusion at the solid–aqueous interface. J. Phys. Chem. Lett. 4, 4064– 4068 (2013).
- A. C. McUmber, T. W. Randolph, D. K. Schwartz, Electrostatic interactions influence protein adsorption (but not desorption) at the silica-aqueous interface. *J. Phys. Chem. Lett.* 6, 2583–2587 (2015).
- 77. K. D. Collins, M. W. Washabaugh, The Hofmeister effect and the behaviour of water at interfaces. *Q. Rev. Biophys.* **18**, 323–422 (1985).
- A. M. Hyde et al., General principles and strategies for salting-out informed by the Hofmeister series. Org. Process Res. Dev. 21, 1355–1370 (2017).
- P. K. Grover, R. L. Ryall, Critical appraisal of salting-out and its implications for chemical and biological sciences. Chem. Rev. 105, 1–10 (2005).
- A. G. Hovanessian, Z. L. Awdeh, Gel isoelectric focusing of human-serum transferrin. Eur. J. Biochem. 68, 333–338 (1976).
- 81. X. Zhang, R. Bai, Adsorption behavior of humic acid onto polypyrrole-coated nylon 6, 6 granules. *J. Mater. Chem.* **12**, 2733–2739 (2002).

- H. Abdizadeh, A. R. Atilgan, C. Atilgan, Mechanisms by which salt concentration moderates the dynamics of human serum transferrin. J. Phys. Chem. B 121, 4778– 4789 (2017).
- X. Zhang, R. Bai, Immobilization of chitosan on nylon 6, 6 and PET granules through hydrolysis pretreatment. J. Appl. Polym. Sci. 90, 3973–3979 (2003).
- R. Walder, M. Kastantin, D. K. Schwartz, High throughput single molecule tracking for analysis of rare populations and events. *Analyst* 137, 2987–2996 (2012).
- T. Ohkuma, S. Hara, Tail-producing slow adsorption—desorption process in liquid solid chromatography. J. Chromatogr. A 400, 47–63 (1987).
- J. T. Cooper, E. M. Peterson, J. M. Harris, Fluorescence imaging of single-molecule retention trajectories in reversed-phase chromatographic particles. *Anal. Chem.* 85, 9363–9370 (2013).
- M. J. Wirth, M. A. Legg, Single-molecule probing of adsorption and diffusion on silica surfaces. *Annu. Rev. Phys. Chem.* 58, 489–510 (2007).
- M. J. Wirth, D. J. Swinton, M. D. Ludes, Adsorption and diffusion of single molecules at chromatographic interfaces. J. Phys. Chem. B 107, 6258–6268 (2003).
- A. Micsonai et al., Accurate secondary structure prediction and fold recognition for circular dichroism spectroscopy. Proc. Natl. Acad. Sci. U.S.A. 112, E3095–E3103 (2015).
- D. F. Marruecos, D. K. Schwartz, J. L. Kaar, Impact of surface interactions on protein conformation. *Curr. Opin. Colloid Interface Sci.* 38, 45–55 (2018).
- M. G. Wyzgoski, G. E. Novak, Stress cracking of nylon polymers in aqueous salt solutions. J. Mater. Sci. 22, 1715–1723 (1987).
- H. S. Gadgil, G. D. Pipes, T. M. Dillon, M. J. Treuheit, P. V. Bondarenko, Improving mass accuracy of high performance liquid chromatography/electrospray ionization time-of-flight mass spectrometry of intact antibodies. J. Am. Soc. Mass Spectrom. 17, 867–872 (2006).
- C. Rivat, P. Sertillanges, E. Patin, J. F. Stoltz, Single-step method for purification of human transferrin from a by-product of chromatographic fractionation of plasma. J. Chromatogr. A 576, 71–77 (1992).
- G. Sawatzki, V. Anselstetter, B. Kubanek, Isolation of mouse transferrin using salting-out chromatography on Sepharose CL-6B. *Biochim. Biophys. Acta* 667, 132– 138 (1981).
- R. Ghosh, Separation of proteins using hydrophobic interaction membrane chromatography. J. Chromatogr. A 923, 59–64 (2001).
- C. Boi, S. Dimartino, G. C. Sarti, Performance of a new protein A affinity membrane for the primary recovery of antibodies. *Biotechnol. Prog.* 24, 640–647 (2008).
- B. B. Langdon et al., Single-molecule resolution of protein dynamics on polymeric membrane surfaces: The roles of spatial and population heterogeneity. ACS Appl. Mater. Interfaces 7, 3607–3617 (2015).
- W. Rieman, 3rd, Salting-out chromatography. A review. J. Chem. Educ. 38, 338–343 (1961).
- F. Dondi, P. Munari, M. Remelli, A. Cavazzini, Monte Carlo model of nonlinear chromatography. Anal. Chem. 72, 4353–4362 (2000).
- 100. A. Cavazzini, F. Dondi, A. Jaulmes, C. Vidal-Madjar, A. Felinger, Monte Carlo model of nonlinear chromatography: Correspondence between the microscopic stochastic model and the macroscopic Thomas kinetic model. *Anal. Chem.* 74, 6269–6278 (2002).
- J. C. Giddings, Dynamics of Chromatography: Principles and Theory (CRC Press, 1965).
- A. Cavazzini, M. Remelli, F. Dondi, A. Felinger, Stochastic theory of multiple-site linear adsorption chromatography. *Anal. Chem.* 71, 3453–3462 (1999).
- 103. Y. Vanderheyden, K. Vanderlinden, K. Broeckhoven, G. Desmet, Problems involving the determination of the column-only band broadening in columns producing narrow and tailed peaks. J. Chromatogr. A 1440, 74–84 (2016).
- 104. A. Felinger, Data Analysis and Signal Processing in Chromatography (Elsevier, 1998).
- 105. F. Gritti, G. Guiochon, Accurate measurements of the true column efficiency and of the instrument band broadening contributions in the presence of a chromatographic column. J. Chromatogr. A 1327, 49–56 (2014).